ARTICLE NO. 78-1167

Detailed Study of Attached and Separated Compression Corner Flowfields in High Reynolds Number Supersonic Flow

Gary S. Settles,* Thomas J. Fitzpatrick,† and Seymour M. Bogdonoff‡
Princeton University, Princeton, N.J.

An experimental study has been carried out to detail the interaction of a compressible turbulent boundary layer with shock waves of varying strengths. The interaction was produced by two-dimensional compression corners of 8, 16, 20, and 24 deg angles. The incoming boundary layer had an edge Mach number of 2.85 and a Reynolds number of 1.7 million based on overall thickness. Detailed mean flow and surface measurements are presented for the four corner angles. The 8 deg corner flow was found to be fully attached, while the 16 deg case was near incipient separation. Both the 20 and 24 deg corners produced significant flow separation regions. In the discussion of these results, emphasis is placed on the development of flowfield properties from attached to separated conditions. Comparisons made with a computational solution of the Navier-Stokes equations show good agreement when the corner flow is not separated. Separated corner flows seem to require a more complex turbulence model in the computational solution.

Nomenclature

C = corner location
C_f = skin friction coefficient
M = Mach number
P = pressure
R = reattachment location
Re = Reynolds number
S = separation location
u = mean velocity component parallel to model surface
x = distance along model surface measured from corner, taken as positive in the downstream direction
x^* = streamwise offset distance
y = distance normal to model surface
α = corner angle, deg
δ = bondary-layer thickness
π = wake component strength parameter

Subscripts

e = boundary-layer edge condition
ℓ = local condition at any point in the flowfield
w = wall
δ = based on δ
0 = initial incoming boundary-layer condition
∞ = initial incoming freestream condition

Introduction

THE interaction of a shock wave and a turbulent boundary layer is a classical problem of fluid mechanics. Such a flow embodies all the difficulties of turbulence, compressibility, and viscous-inviscid interaction phenomena. It has, in addition, practical importance in such areas as inlet design, external aerodynamics, and turbomachinery. Since no theoretical solution for this problem has been developed, shock boundary-layer interaction experiments continue in order to provide further insight on the phenomenon, and to support modern computational and turbulence modeling efforts.

The present study is part of an ongoing experimental program at Princeton University in both two- and three-dimensional shock boundary-layer interactions.[1-4] Specifically, this paper concerns the two-dimensional interactions generated by compression corners of varying strengths. Four compression corner flowfields are examined by way of detailed mean flow and surface measurements. The comparison of attached and separated flowfield conditions is stressed in the discussion of results. Finally, a comparison is also made with computational solutions of the Navier-Stokes equations using one of many available assumed-turbulence models.

Experimental Procedures

A completed documentation of the experimental procedures used in this study is available in previous publications.[2-5] The present discussion is abridged accordingly.

This investigation was carried out in the Princeton University 20×20 cm high Reynolds number channel. The 8, 16, 20, and 24 deg compression corner models were tested consecutively on the wall of the channel, as illustrated in Fig. 1. The uniform freestream airflow conditions were: Mach number = 2.85, stagnation pressure = 6.8 atm, stagnation temperature = 268 K $\pm 6\%$, and average freestream unit Reynolds number = 7.3×10^7/m.

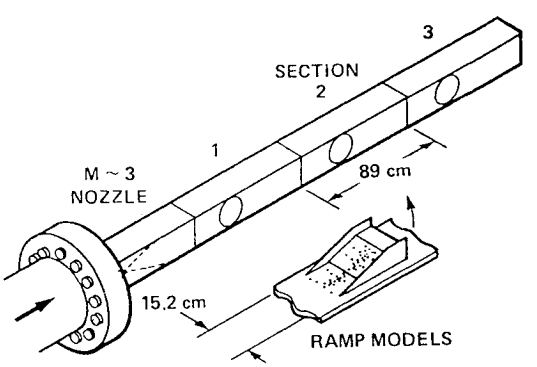

Fig. 1 Sketch of the 20×20 cm high Reynolds number channel and test model installation.

Received July 5, 1978. Presented as Paper 78-1167 at the AIAA 11th Fluid and Plasma Dynamics Conference, Seattle, Wash., July 10-12, 1978; revision received Jan. 29, 1979.

Index categories: Supersonic and Hypersonic Flow; Boundary Layers and Convective Heat Transfer—Turbulent; Shock Waves and Detonations.

*Research Staff Member, Gas Dynamics Lab., Dept. of Mechanical and Aerospace Engineering. Member AIAA.

†Graduate Research Assistant, Gas Dynamics Lab., Dept. of Mechanical and Aerospace Engineering.

‡Professor and Chairman, Dept. of Mechanical and Aerospace Engineering. Fellow AIAA.

The incoming turbulent boundary layer for the four compression corner experiments has an overall thickness, δ_0, of about 2.3 cm. The boundary layer is in an equilibrium condition, with zero pressure gradient and near-adiabatic wall conditions.[5] It is closely matched by the compressible flow wall-wake law[7,8] with a wake strength parameter π of 0.55.

The measurements carried out during the compression corner experiments include detailed probe[2] surveys of pitot and static pressures and total temperature throughout each interaction flowfield. Surface static pressure measurements and Preston tube readings were also taken. Flow visualization techniques included shadowgraph and color Schlieren optics and surface streak patterns.

Probe interference with the flowfields under study was checked and found not to be a significant problem. Along similar lines, a search for evidence of unsteadiness in the mean flowfield scales (e.g., shock positions and flow separation lengths) revealed no excursions greater than 10% of δ_0. An examination of flowfield two-dimensionality is treated in a later section.

Measured profiles of static and pitot pressure and total temperature were combined to derive mean streamwise Mach number and velocity profiles. The accuracies of these derived quantities are believed to be within $\pm 3\%$ and $\pm 5\%$, respectively, except in the immediate vicinity of compression waves.

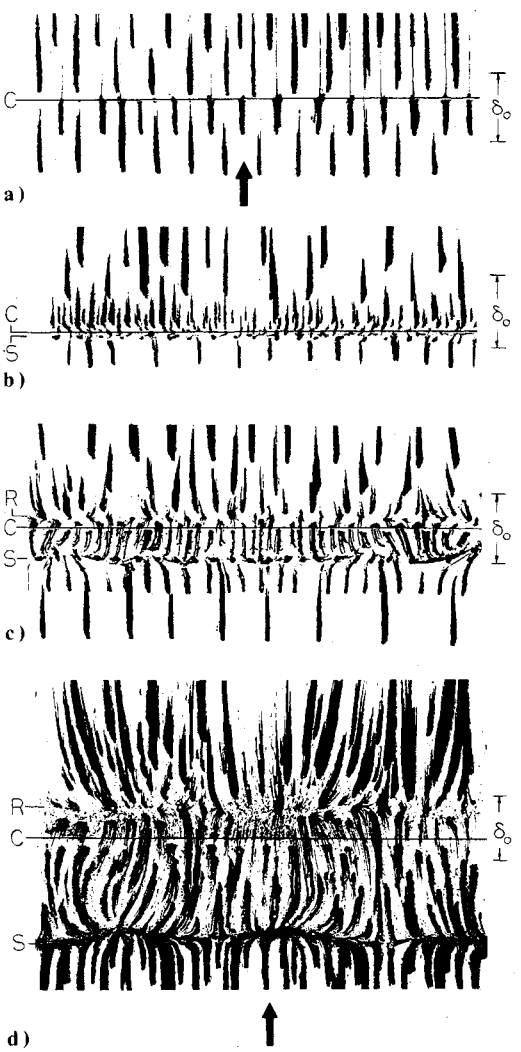

Fig. 2a-d Surface streak patterns from the 8, 16, 20 and 24 deg compression corner flowfields. (S, C, and R denote separation, corner, and reattachment locations, respectively. The streamwise direction is from bottom to top in each case. The incoming boundary-layer thickness is shown for comparison.)

Experimental Results

Surface Flow Patterns

An overall view of the development of the compression corner flow with increasing corner angle is given by the surface streak patterns of Fig. 2. These streak patterns were obtained by applying a thick mixture of graphite powder and

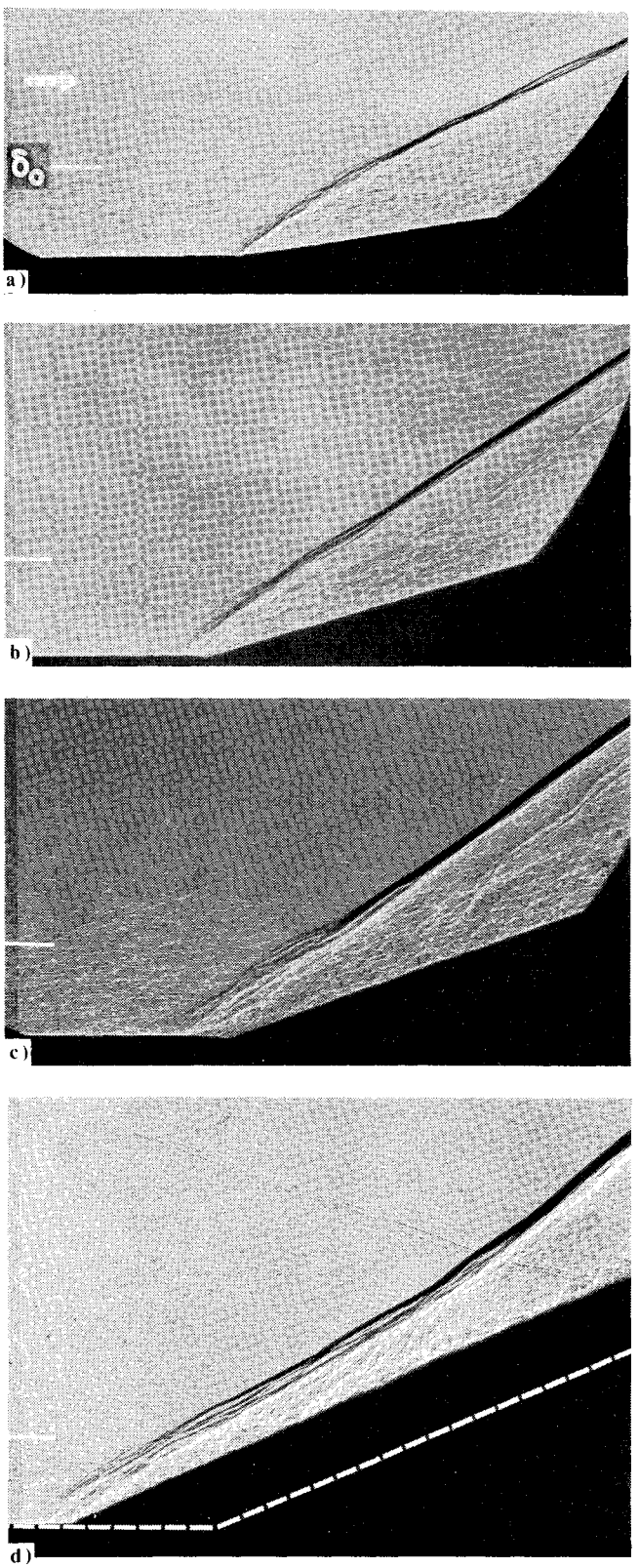

Fig. 3a-d Flowfield shadowgrams of the 8, 16, 20, and 24 deg interactions. (Flow is from left to right in each case; the location of the 24 deg model surface is shown by a broken line.)

silicone oil to the model surface in discrete dots prior to a test run. The patterns were lifted off the surface and preserved after a test by the use of transparent adhesive tape.

The streaks cross the compression corner in the 8 deg case with no discernible flow separation. At 16 deg, however, evidence of a separation line appears just upstream of the corner. At the 20 deg corner angle, this separated region has grown to the extent of about 65% of δ_0. At the largest corner angle tested, 24 deg, the extent of the separated region, as measured along the model surface, is slightly more than twice the incoming boundary-layer thickness.

The compression corner flowfield is thus seen to progress from the fully attached condition to a condition of significant flow separation over the range of corner angles tested. The separation and reattachment locations, as well as the flow reversal near the surface, are clearly illustrated by the streaklines in the 20 and 24 deg cases. The present indication of incipient separation at a corner angle near 16 deg is in close agreement with the results of the authors' previously published study of incipient separation at Mach 3 and high Reynolds numbers.[1]

Optical Flow Visualization

Microsecond spark shadowgrams of the four corner flows are shown in Fig. 3. A distinct shock wave is seen to arise from the corner location in the 8 deg case. The 16 and 20 deg shadowgrams are characterized by an increasing upsteam influence of the compression corner, and by the spreading of the shock wave into a compression fan within the boundary layer. For $\alpha = 24$ deg, a large upsteam influence and the dual character of the shock system are apparent. In this case the flow undergoes an initial turn at separation and generates a shock wave. An additional compression fan at reattachment merges with the separation shock and reinforces it. This dual compression wave system is a clear indication of the presence of flow separation at a compression corner.[1] Part of the 24 deg corner shadowgram in Fig. 3d is obscured by the aerodynamic fences which were necessary to insure flowfield two-dimensionality.

Surface Pressure Distributions

The surface static pressure distributions on the four compression corner models are shown in Fig. 4. The upstream influence of the compression corner is seen to range from a small fraction of δ_0 in the 8 deg case to about two δ_0 in the 24 deg case. The distributions for the two larger corner angles exhibit well-defined "kinks," another indication of the presence of flow separation.[9,1] The separation and reattachment locations for the 24 deg corner and the separation location for the 20 deg corner are noted in Fig. 4. Also shown are the theoretical inviscid pressure-rise levels for the four test cases. These are closely matched by the data for all cases except 24 deg, wherein the pressure taps did not extend far enough downstream to record the pressure level-off. However, checks[2] were made to insure that the 24 deg ramp length was enough to approximate infinite ramp conditions.[10]

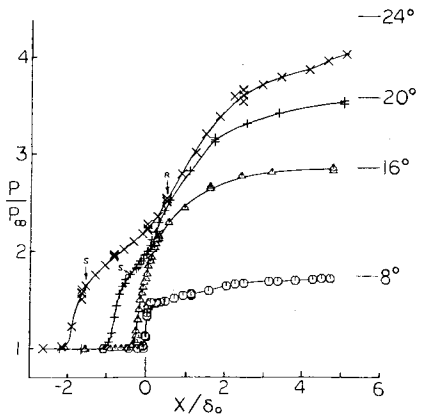

Fig. 4 Surface pressure distributions on the 8, 16, 20, and 24 deg compression corner models.

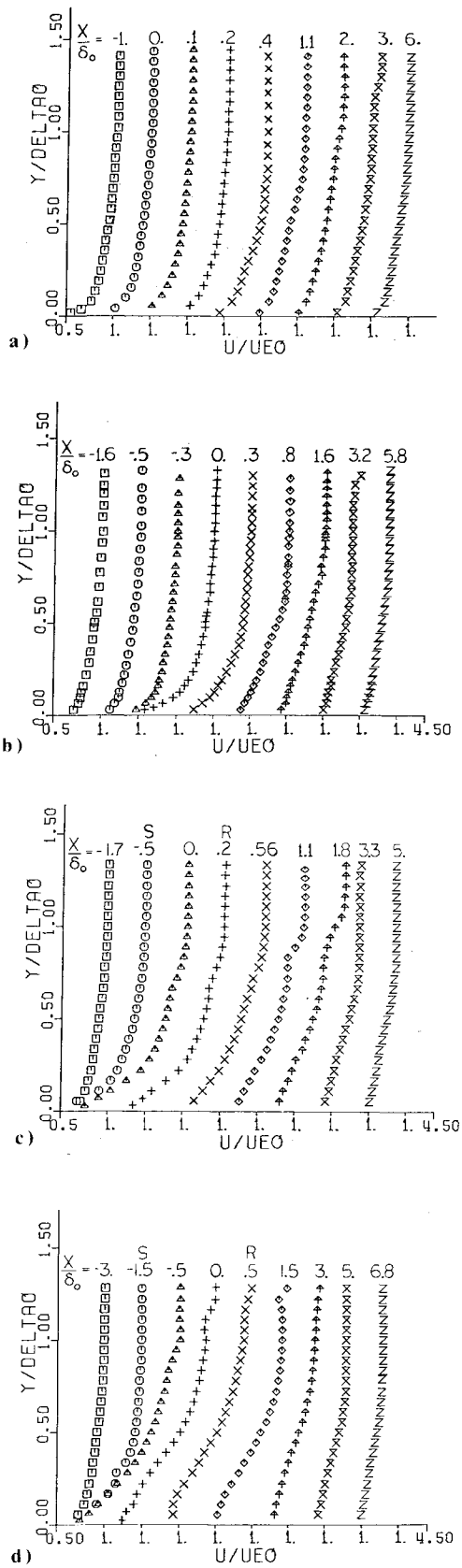

Fig. 5a-d Selected mean streamwise velocity profiles from the 8, 16, 20, and 24 deg compression corner flowfields.

Velocity Profiles

Mean streamwise velocity profiles were obtained at many stations throughout each of the four compression corner flowfields, including some reverse-flow profiles in the 20 and 24 deg separated regions. The 20 and 24 deg velocity profiles have been reported previously in some detail.[11,2,5] The amounts of data obtained in the investigation preclude any quantitative presentation here, but detailed profile tabulations are available directly from the authors.

In this light, a selection of nine velocity profiles from each compression corner flowfield is shown in Figs. 5a-d. These plots serve to illustrate the changes in boundary-layer velocity profiles which occur along the length of each interaction flowfield. The first profile in each series is that of the incoming equilibrium turbulent boundary layer. Appropriate x/δ_0 stations are indicated for each velocity profile shown.

Mild flow retardation for the 8 deg corner flow (Fig. 5a) progresses toward severe retardation with flow reversal in the 24 deg case (Fig. 5d). The location of the shock system appears as a kink in some velocity profiles downstream of the compression corner location. These downstream profiles are seen to recover rapidly from the retarding effects of the imposed adverse pressure gradients. The rate and extent of this recovery is discussed more fully in later sections.

Skin Friction Results

The skin friction distributions on the four compression corner models, as obtained by the Preston tube technique, are shown in Fig. 6. This estimation of C_f from Preston tube readings in an adverse pressure gradient required the assumption of "effective" local boundary-layer edge conditions based on tunnel stagnation and local static pressures. Although the resulting C_f values are somewhat approximate, excellent agreement is found between the zero skin friction points shown in Fig. 6 and the flow separation and reattachment points determined by other methods. Also, the data of Fig. 6 closely match the incoming boundary-layer C_f value given by the Van Driest II transformation.[12] Also shown in Fig. 6 are estimated downstream equilibrium C_f levels obtained from the Van Driest II transformation at the downstream flow conditions for the four compression corners. The skin friction results appear to match these levels reasonably, although C_f is still rising somewhat at the downstream end of each experimental flowfield.

Discussion and Comparison of Results

Numerical Simulation

The experimental flowfields described here have been simulated by numerical computations carried out at the NASA Ames Research Center.[11,13] These solutions were obtained on a high-speed computer using several different assumed-turbulence models for closure of the time-averaged compressible Navier-Stokes equations. Specifically, these turbulence models were an algebraic eddy viscosity function, a model using an additional partial differential equation for the kinetic energy of turbulence, and a model using still another partial differential equation for the turbulence length scale. Referred to as the zero-, one-, and two-equation models, all three amount to successively more complex representations of the eddy viscosity concept. The details of these models are available in several publications (e.g., Ref. 13), and are not recounted here.

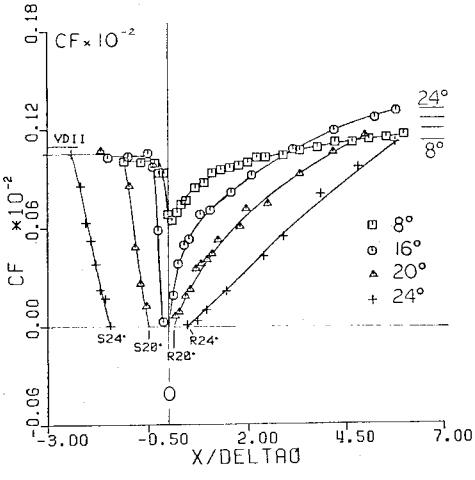

Fig. 6 Distributions of skin friction coefficient for the 8, 16, 20, and 24 deg compression corners.

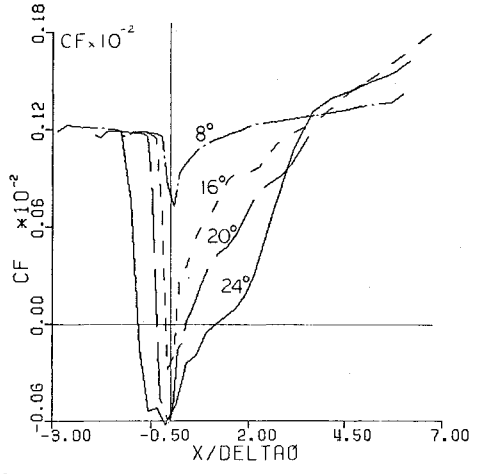

Fig. 7 Computed skin friction distributions for the four compression corners.

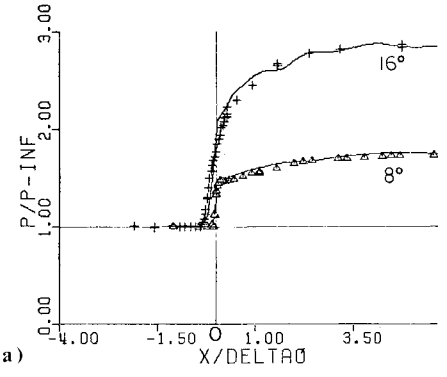

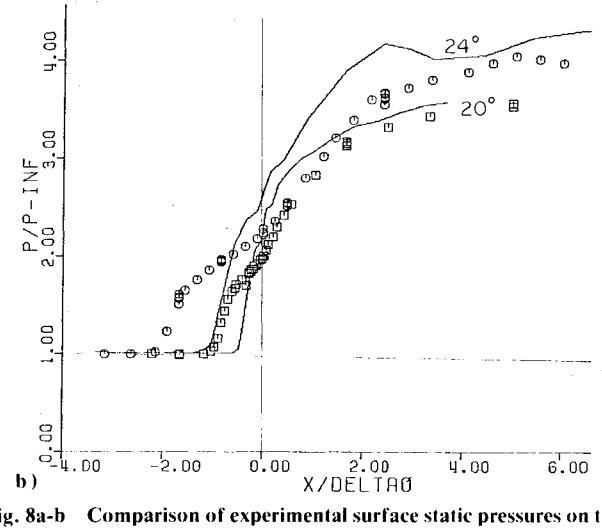

Fig. 8a-b Comparison of experimental surface static pressures on the four compression corner models with computations using a one-equation turbulence model.

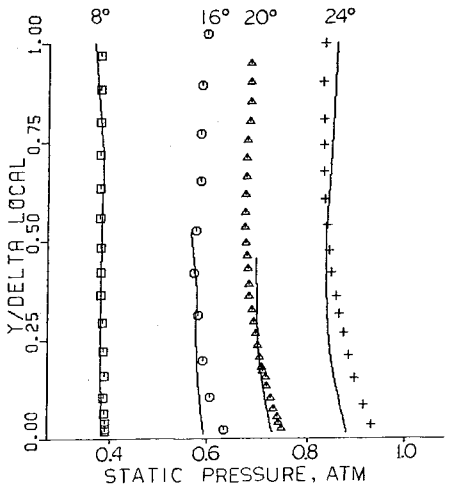

Fig. 9 Comparison of experimental and computed downstream static pressure profiles for the four compression corner flowfields. (Profile locations are at $x/\delta_0 \simeq 5$ for $\alpha = 8$, 16, and 24 deg and $x/\delta_0 = 2.75$ for $\alpha = 20$ deg.)

Comparisons of the computed results with the present experimental data showed that the three turbulence models all lead to similar results, in that certain features of the experiment were predicted and others were not. Overall, the one-equation model may have done slightly better than the others, though the distinction is by no means clear. Under these circumstances, and to avoid confusion in the plotted comparisons, solutions using this model are the only ones illustrated. The conclusions of this paper hold for all three turbulence models.

Some comparisons of the 20 and 24 degree experimental data and computations have already been published.[11,13,22] These comparisons will not be repeated in detail here.

Skin Friction Comparison

Figure 7 shows the computed skin friction distributions on the four compression corners plotted to the same scale as the experimental data in Fig. 6. While the 8 and 16 deg experimental and computed C_f distributions are in reasonable agreement, the experiment and the computation disagree concerning separation and reattachment locations at the higher (separated) corner angles. Further, the computed outgoing C_f values are generally higher than the experimental values for all corner angles.

Surface Pressure Distributions

The computed and experimental surface static pressure distributions on the compression corner models are shown in Figs. 8a and 8b. The agreement of the one-equation model results with the 8 and 16 deg corner data in Fig. 8a is excellent. However, Fig. 8b shows that the computational predictions of the 20 and 24 deg surface pressure data are not good. This striking contrast is believed to reflect an inadequacy of the turbulence modeling schemes where significant flow separation is involved (as it is in the 20 and 24 deg data, but not in the 8 and 16 deg data). Similar comparisons were drawn using computations with zero- and two-equation turbulence models, yielding the same overall conclusion.

Downstream Static Pressure Profiles

The experimental boundary-layer static pressure profiles for the 16, 20, and 24 deg compression corners reveal a lingering normal static pressure gradient in the boundary layer emerging from the interaction. As shown in Fig. 9, the static presure decreases about 10% from the model surface to the boundary-layer edge for the three higher corner angle cases, but is essentially constant for the 8 deg corner case.

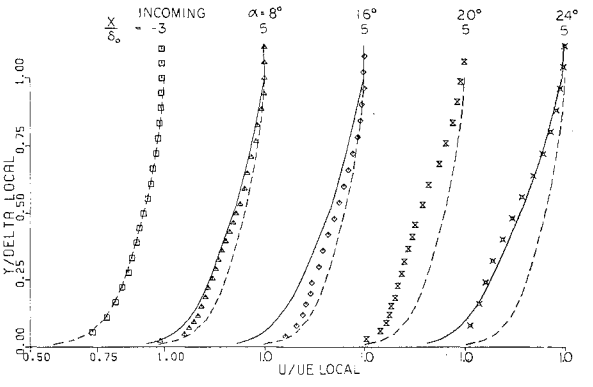

Fig. 10 Comparison of outgoing velocity profiles for the four ramp angles with computed profiles and estimated downstream equilibrium profiles. (—Navier-Stokes solution with one-equation model; --- Equilibrum wall-wake profile with $\pi = 0.55$)

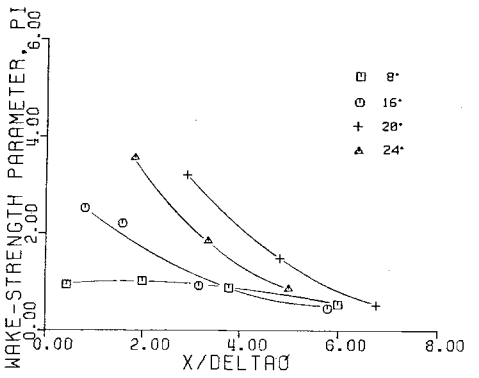

Fig. 11 Decay of the velocity profile wake-strength parameter with distance downstream of each compression corner.

This phenomenon is predicted, to some extent by the computational results also shown in Fig. 9. It is believed that these downstream normal static pressure gradients are produced by waves which are remnants of the interaction at the compression corner.

The needle-type static pressure probe used to make the measurements shown in Fig. 9 indicates a constant static pressure equal to the wall value when checked in the incoming equilibrium turbulent boundary layer. An approximate check on the streamline curvature in the outgoing boundary layers reveals insufficient curvature to account for the measured static pressure gradient on the basis of any probe misalignment error.

Outgoing Velocity Profiles

In order to examine the recovery of the boundary-layer velocity profiles downstream of the four compression corner interactions, the outgoing velocity profiles at the $x/\delta_0 \simeq 5$ stations of each ramp are compared in Fig. 10. Also shown in the figure are estimates of the downstream equilibrium profile shape from the compressible wall-wake law.[7] The incoming equilibrium profile and its wall-wake representation are additionally shown for comparison. In each case, the wall-wake law is evaluated with the Coles[8] equilibrium wake-strength value of $\pi = 0.55$.

The solid lines in Fig. 10 are the computed profiles from the Navier-Stokes solution, which are shown for every profile except that of the 20 deg corner, since the computation did not extend to $x/\delta_0 = 5$ in that case. The incoming velocity profile is closely matched by both the computed solution and the wall-wake law. The 8 deg corner outgoing profile agrees with the computation, but has not yet reached equilbrium by comparison with the wall-wake law. As the corner angle is increased, the experimental profiles are seen to be increasingly

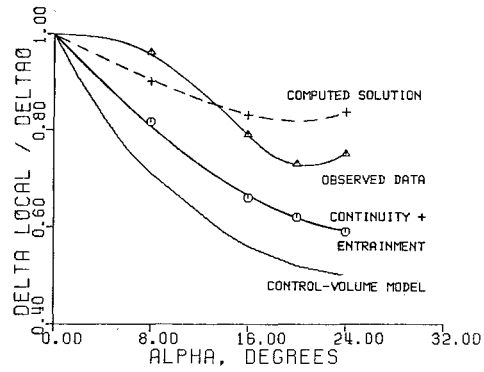

Fig. 12 Overall boundary-layer thickness vs α at $x/\delta_0 \simeq 5$.

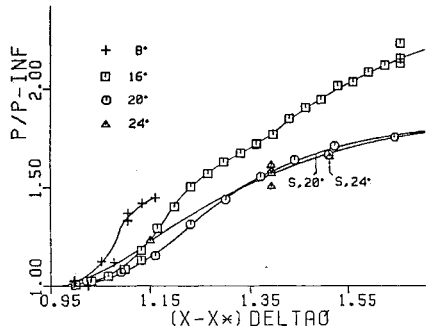

Fig. 13 Initial surface pressure rise data for the 8, 16, 20, and 24 deg compression corners.

retarded compared to the equilibrium representation of the wall-wake law. In each outgoing case, the experimental velocity profile of Fig. 10 exhibits a more pronounced inflection in the region $0.25 < y/\delta_\ell < 0.75$ than is predicted by either the computed solution or the equilibrium wall-wake law. In general, the present computed solution using a one-equation turbulence model is in reasonable agreement with the experimental outgoing velocity profiles. This was not the case, however, for three other turbulence models which were compared with the 20 and 24 deg data in Ref. 11.

Velocity Profile Recovery in the Relaxation Zone

It was shown in Figs. 5a-d that the velocity profiles rapidly relax toward equilibrium downstream of the compression corner. To examine this in more detail, the combined wall-wake law for turbulent boundary layers was matched to the experimental profiles using a least-squares curvefit.[7] Resulting values of the velocity profile wake-strength parameter, π, are plotted vs x/δ_0 for the four compression corner models in Fig. 11. As expected, strong wake components are found just downstream of the compression corner for all angles except 8 deg, indicating large velocity deficits between the logarithmic region and the boundary-layer edge. Further, the velocity profiles are seen to relax rapidly toward an equilibrium π value of roughly 0.5 with incrasing x/δ_0. (To avoid oversimplification, it should be noted that the equilibrium value of π may be a function of downstream Mach and Reynolds numbers,[14,8] so 0.55 is by no means a universal value.)

Outgoing Boundary-Layer Thickness

Overall boundary-layer thicknesses throughout each compression corner interaction were determined at $0.99\, u_{e_\ell}$. These are plotted versus corner angle at the downstream $x/\delta_0 \simeq 5$ station in Fig. 12. For comparison, the computed Navier-Stokes solution and the prediction of a simple control-volume technique[23] are also shown. The computed outgoing δ is seen to be somewhat thicker than the experimental δ for $\alpha = 20$ and 24 deg. The control-volume technique also predicts the general trend of the results but seriously underestimates them in magnitude.

As a further check, the mean flow continuity equation was used with the measured profiles to trace the path of the incoming boundary-layer edge streamline through each interaction. At $x/\delta_0 \simeq 5$, the heights of these streamlines were multiplied by a factor of 1.07 to account in an approximate way for flat-plate mass entrainment over the length of the compression corner models. As shown in Fig. 12, this technique underpredicts the measured boundary-layer thicknesses by about 20%. Thus, the outgoing boundary layers are considerably thicker than can be accounted for on the basis of the zero-pressure-gradient entrainment phenomenon. The effect of the shock wave interaction swells these layers, probably due to a much more violent mixing phenomenon within the interaction than that which occurs in a flat-plate boundary layer.

Two-Dimensionality

The two-dimensionality of the 8 and 16 deg compression corner flowfields was proved in Refs. 1 and 5 by a comparison with similar tests carried out on an axisymmetric body. Comprehensive efforts were made to insure the two-dimensionality of all four corner flows by the careful application of aerodynamic fences (Ref. 5, Appendix C). The results indicate two-dimensionality in terms of insignificant measured spanwise pressure variations and essentially straight separation and reattachment lines. Nevertheless, no absolute proof can be made of the two-dimensionality of the 20 and 24 deg flowfields. The 24 deg surface streak pattern of Fig. 2d exhibits a symmetrical "node and saddle point" behavior which has been noticed by several investigators[15-17] in otherwise two-dimensional flows, and has been the subject of at least one theoretical study.[18]

Approach to a Free Interaction

The free interaction concept, originally proposed by Chapman, et al.,[19] has been verified by many investigators of supersonic shock wave boundary-layer interactions, (e.g., Refs. 20 and 21). In essence, this concept states that the viscous-inviscid interaction up to a point of boundary-layer separation is independent of the downstream device which provokes the separation. Free-interaction has been checked in the present experiment by plotting the surface pressure data for the four compression corner experiments on an offset scale so that the initial points of pressure rise are coincident. This plot is shown as Fig. 13. It illustrates that the initial slope of the pressure rise decreases with increasing α until a constant, free-interaction value is reached. Only the 20 and 24 deg corner angles produce sufficiently large separated regions to achieve this value. The pressure distributions for the latter two corner angles are in good agreement up to and beyond the separation locations, which also agree well.

Concluding Remarks

In summary, an experimental study is reported concerning the shock wave turbulent boundary-layer interaction generated by two-dimensional compression corners of 8, 16, 20, and 24 deg angles. The incoming boundary layer has an edge Mach number of 2.85 and a Reynolds number of 1.7×10^6 based on overall thickness. Detailed surface and mean flowfield data are presented. Results indicate that the range of corner angles studied produces an interaction flowfield which progresses from fully attached conditions through incipient separation to significantly separated conditions.

A detailed comparison is made with a computational solution of the Navier-Stokes equations using an assumed one-equation turbulence model. The results of this comparison show that many features of the experimental flowfields are adequately predicted by the computation, but

that the poorest match between the computation and experiment occurs in cases where flow separation is present. The essential features of an attached-flow interaction are adequately represented by the inviscid character of the computational solution. Significant discrepancies only occur in the separated flow cases where the turbulence phenomenon is not adequately modeled in the numerical computation. For the one-equation turbulence model tested here, some flowfield features (e.g., outgoing velocity profiles) are predicted by the computation, while others (e.g., separation and reattachment locations) are not. Similar conclusions were reached for computations using zero- and two-equation turbulence models.

A normal gradient in flowfield static pressure is found in the outgoing boundary layers of the 16, 20, and 24 deg compression corners. This gradient appears to be due to waves which are remnants of the interaction at the compression corner.

The mean velocity profiles immediately downstream of each compression corner are highly retarded. However, these profiles exhibit a rapid recovery toward equilibrium with increasing downstream distance. None of the outgoing profiles have reached equilibrium by $5\delta_0$ downstream of the corner location.

The present study is part of a continuing program being carried out at the Gas Dynamics Laboratory of Princeton University. An effort to obtain turbulence fluctuation measurements and direct heat-transfer readings in high Reynolds compression corner flowfields is currently under way. The study of three-dimensional shock/boundary-layer interactions is also a major part of this program.

Acknowledgements

This work was supported by the Air Force Office of Scientific Research under Contract F44620-75-C-0080 and by NASA Ames Research Center under Grant NSG-2114. The assistance of C.C. Horstman of NASA-Ames in supplying the numerical computations is gratefully acknowledged.

References

[1] Settles, G.S., Bogdonoff, S.M., and Vas, I.E., "Incipient Separation of a Supersonic Turbulent Boundary Layer at High Reynolds Numbers," *AIAA Journal,* Vol. 14, Jan. 1976, pp. 50-56.

[2] Settles, G.S., Vas, I.E., and Bogdonoff, S.M., "Details of a Shock-Separated Turbulent Boundary Layer at a Compression Corner," *AIAA Journal,* Vol. 14, Dec. 1976, pp. 1709-1715.

[3] Oskam, B., Vas, I.E., and Bogdonoff, S.M., "Mach 3 Oblique Shock Wave/Turbulent Boundary Layer Interaction in Three Dimensions," AIAA Paper 76-336, July 1976.

[4] Dolling, D.S., Cosad, C.D., and Bogdonoff, S.M., "Three-Dimensional Shock Wave Turbulent Boundary Layer Interactions—A Parametric Study of Blunt Fin-Induced Flows," AIAA Paper 78-159, Jan. 1978.

[5] Settles, G.S., "An Experimental Study of Compressible Turbulent Boundary Layer Separation at High Reynolds Number," Ph.D. Dissertation, Aerospace and Mechanical Sciences Dept., Princeton University, Princeton, N.J., Sept. 1975.

[6] Vas, I.E. and Bogdonoff, S.M., "A Prelimnary Report on the Princeton University 8″ × 8″ Supersonic Tunnel," Internal Memo. 39, Gas Dynamics Lab., Dept. of Aerospace and Mechanical Sciences, Princeton University, 1971.

[7] Mathews, D.C., Childs, M.E., and Paynter, G.C., "Use of Coles' Universal Wake Function for Compressible Turbulent Boundary Layers," *Journal of Aircraft,* Vol. 7, No. 2, March-April 1970, pp. 137-140.

[8] Coles, D.E., "The Turbulent Boundary Layer in a Compressible Fluid," Rand Corporation Rept. R-403-PR, 1962.

[9] Kuehn, D.M., "Experimental Investigation of the Pressure Rise Required for the Incipient Separation of Turbulent Boundary Layers in Two-Dimensional Supersonic Flow," NASA Memo 1-21-59A, 1959.

[10] Hunter, L.G., and Reeves, B.L., "Results of a Strong Interaction Wake-Like Model of Supersonic Separated and Reattaching Turbulent Flows," *AIAA Journal,* Vol. 9, April 1971, pp. 703-712.

[11] Horstman, C.C., Settles, G.S., Vas, I.E., Bogdonoff, S.M. and Hung, C.M., "Reynolds Number Effects on Shock-Wave Turbulent Boundary Layer Interactions," *AIAA Journal,* Vol. 15, Aug. 1977, pp. 1152-1158.

[12] Van Driest, E.R., "The Problem of Aerodynamic Heating," *Aerospace Engineering Review,* Vol. 15, Oct. 1956, pp. 26-41.

[13] Coakley, T.J., Viegas, J.R., and Horstman, C.C., "Evaluation of Turbulence Models for Three Primary Types of Shock Separated Boundary Layers." AIAA Paper 77-692, June 1977.

[14] Baronti, P.O. and Libby, P.A., "Velocity Profiles in Turbulent Compressible Boundary Layers," *AIAA Journal,* Vol. 4, Feb. 1966, pp. 193-202.

[15] Ginoux, J., "On the Existence of Cross Flows in a Separated Supersonic Stream," TCEA TN6, 1962.

[16] Roshko, A. and Thomke, G.J., "Flare-Induced Separation Lengths in Supersonic, Turbulent Boundary Layers," *AIAA Journal,* Vol. 14, July 1976, pp. 873-879.

[17] Simpers, G., Vas, I.E., and Bogdonoff, S.M., "Turbulent Shear Layer Reattachment at M ~ 3," AIAA Paper 77-43, Jan. 1977.

[18] Inger, G.R., "Three-Dimensional Disturbances in Reattaching Separated Flows," in AGARD-CPP-168, *Flow Separation,* 1975.

[19] Chapman, D.R., Kuehn, D.M., and Larson, H.K., "Investigation of Separated Flows in Supersonic Stream with Emphasis on the Effect of Transition," NACA Rept. 1356, 1958.

[20] Zukoski, E.E., "Turbulent Boundary-Layer Separation in Front of a Forward-Facing Step," *AIAA Journal,* Vol. 5, Oct. 1967, pp. 1746-1753.

[21] Law, C.H., "Two-Dimensinal Compression Corner and Planar Shock Wave Interactions with a Supersonic, Turbulent Boundary Layer," USAF ARL Rept. 0157, June 1975.

[22] Viegas, J.R. and Horstman, C.C., "Comparison of Multiequation Turbulence Models for Several Shock-Separated Boundary-Layer Interaction Flows," AIAA Paper 78-1165, July 1978.

[23] Kotansky, D.R., "Application of Transformation Methods to Wedge-Shock/Boundary-Layer Interactions," *AIAA Journal,* Vol. 9, April 1971, pp. 731-733.